

# We are IntechOpen, the world's leading publisher of Open Access books Built by scientists, for scientists

6,900

Open access books available

186,000

International authors and editors

200M

Downloads

Our authors are among the

154

Countries delivered to

TOP 1%

most cited scientists

12.2%

Contributors from top 500 universities



WEB OF SCIENCE™

Selection of our books indexed in the Book Citation Index  
in Web of Science™ Core Collection (BKCI)

Interested in publishing with us?  
Contact [book.department@intechopen.com](mailto:book.department@intechopen.com)

Numbers displayed above are based on latest data collected.  
For more information visit [www.intechopen.com](http://www.intechopen.com)



---

# Multiple-Input Multiple-Output (MIMO) Optical Wireless Communications

---

Oswaldo González

Additional information is available at the end of the chapter

<http://dx.doi.org/10.5772/46079>

---

## 1. Introduction

People's ideas about communications have changed completely, nowadays when this subject is mentioned almost everyone thinks of wireless communications. The demand for broadband wireless communications offering greater and greater data rates is endless, and the radio-technology community is trying harder and harder to satisfy this demand. Recently, there was the worldwide launch of 4<sup>th</sup> generation (4G) systems promising 100 Mbit/s for high mobility communications and up to 1 Gbit/s for stationary or low mobility communications. The key to this technology is the combination of orthogonal frequency-division multiple access (OFDMA) applied to multiple-input multiple-output (MIMO) systems.

On the other hand, researchers in wireless optical communications (WOC) are trying to find a way to gain the interest of communication companies by providing new and attractive alternatives to radio communications, as we must not lose sight of the fact that most wireless communications are established inside rooms. Thus, WOC systems offer some advantages over their radio-frequency (RF) counterparts [15]: they are, theoretically, unregulated and have unlimited<sup>1</sup> bandwidth. There is also an inherent security capability, as light (communication) is confined to the room, and there is immunity to multipath fading. However, they are not exempt from drawbacks: strict power limitations due to eye-safety constraints, severe path losses and multipath dispersion and, last but not least, limited maximum achievable signal-to-noise ratio (SNR) due to unavoidable natural and artificial noise sources are the main problems.

Over the last few years, OFDM has begun to be proposed for both fibre and wireless optical communications [4] as an effective solution to mitigating inter-symbol interference (ISI) caused by dispersive channels. Furthermore, the frequency-domain channel equalization provided by an OFDM system does not undergo severe complexity penalty when data rates and dispersion increase as opposed to serial time-domain equalizers, and MIMO techniques can be applied to these systems with relative ease. Finally, the complexity of transmitters

---

<sup>1</sup> This is not strictly true for new visible-light communication (VLC) systems, where LEDs present a transmission bandwidth limited to several MHz

and receivers is transferred from an analogue to a digital domain by employing Fast Fourier Transform (FFT) and Inverse FFT (IFFT) blocks as demodulators and modulators, respectively. Therefore, all these aspects favour the implementation of OFDM systems in the current digital era.

This chapter describes the characteristics of MIMO-OFDM systems applied to WOC, discussing their benefits, but also their drawbacks, as compared with other techniques used in order to obtain high-capacity optical data networks.

## 2. The optical channel model

In wireless optical communications, the optical link is typically established by means of *optical modulation* (IM), in which the desired waveform is modulated onto the instantaneous power of the carrier, in conjunction with *direct detection* (DD) as a down-conversion technique at the receiver end. Therefore, the transmitted waveform  $x(t)$  is the instantaneous optical power of the emitter, and the received waveform  $y(t)$  is the instantaneous current in the receiving photodetector. In this way, the optical channel with IM/DD can be modelled as a *baseband* linear system with impulse response  $h(t)$  or, alternatively, this can be described in terms of the frequency response:

$$H(f) = \int_{-\infty}^{\infty} h(t)e^{-j2\pi ft} dt \quad (1)$$

which is the Fourier transform of  $h(t)$ . This channel model  $h(t)$  is practically stationary because it only varies when emitter, receiver or objects in the room are moved by tens of centimetres. In many applications, optical links are operated in the presence of intense infrared and visible background light. The received background light adds shot noise, which is usually the limiting noise source in a well-designed receiver. Due to its high intensity, this shot noise can be modelled as white, Gaussian, and independent of  $x(t)$ . When little or no ambient light is present, the dominant noise source is receiver preamplifier noise, which is also signal-independent and Gaussian (though often nonwhite) [15]. Thus, the noise  $n(t)$  is usually modelled as Gaussian and signal-independent, and the instantaneous output current at the receiver can be represented as:

$$y(t) = Rx(t) \otimes h(t) + n(t) \quad (2)$$

where the “ $\otimes$ ” symbol denotes convolution and  $R$  is the detector responsivity (A/W). According to (2), the optical link can be completely characterized by means of the impulse response  $h(t)$  and the noise sources  $n(t)$ . The knowledge of  $h(t)$  allows us to determine the multipath penalty, which limits the maximum baud rate. The second term is related to the signal-to-noise ratio (SNR), which determines the performance of the digital link.

In order to evaluate the impulse response on indoor wireless optical channels, several deterministic methods were first proposed [5]. However, these methods can only be implemented to determine the impulse response until the third reflection due to their computational complexity. Later on, modified Monte Carlo-based ray-tracing algorithms were introduced, which present a lower computational cost and without limit to the number of reflections being considered [10].

In these algorithms, ray directions are randomly generated according to the radiation pattern from the emitter. The contribution of each ray from the source or after a bounce to the receiver is computed deterministically. Consequently, the discretisation error is due to the number of

random rays. The line-of-sight (LOS) and multiple-bounce impulse responses are considered when calculating the total impulse response.

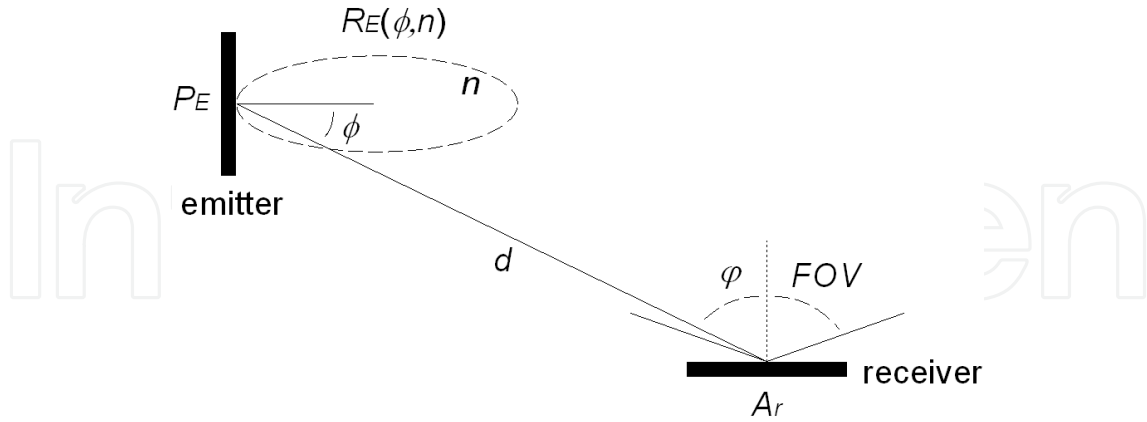


**Figure 1.** LOS contribution to the total received power

## 2.1. LOS impulse response

Given an emitter  $E$  and receiver  $R$  in an environment without reflectors (see Fig. 1), with a large distance  $d$  between both, the received power is approximately:

$$P_R = \frac{1}{d^2} R_E(\phi, n) A_{\text{eff}}(\phi) \quad (3)$$

where the emitter is modelled using a generalized Lambertian radiation pattern  $R_E(\phi, n)$ .  $A_{\text{eff}}(\phi)$  represents the effective signal collection area of the receiver.

$$R_E(\phi, n) = \frac{n+1}{2\pi} P_E \cos^n(\phi), \quad 0 \leq \phi \leq \frac{\pi}{2} \quad (4)$$

$$A_{\text{eff}} = A_r \cos \phi \text{rect}\left(\frac{\phi}{\text{FOV}}\right) \quad (5)$$

$$\text{rect}(x) = \begin{cases} 1, & |x| \leq 1 \\ 0, & |x| > 1 \end{cases} \quad (6)$$

Here  $n$  is the *order* or *mode number* of the radiation lobe that specifies the directionality of the emitter,  $P_E$  the power radiated by the emitter,  $A_r$  the physical area of the receiver, and FOV the receiver field of view (half-angle from the surface normal).

## 2.2. Multiple-bounce impulse response

If we now consider an emitter  $E$  and receiver  $R$  in a room with reflectors, the radiation from the emitter can reach the receiver after any number of reflections (see Fig. 2). In the algorithm, many rays are generated at the emitter position with a probability distribution equal to its normalized radiation pattern  $R_E(\phi, n) / P_E$ . The power of each generated ray is initially  $P_E / N$ , where  $N$  is the number of rays used to discretise the source. When a ray impinges on a surface, the reflection point is converted into a new optical source, thus, a new ray is generated with a probability distribution provided by the reflection pattern of that surface,  $R_S(\theta, \theta')$ . The process continues during the simulation time  $t_{\text{max}}$ . After each reflection, the power is reduced

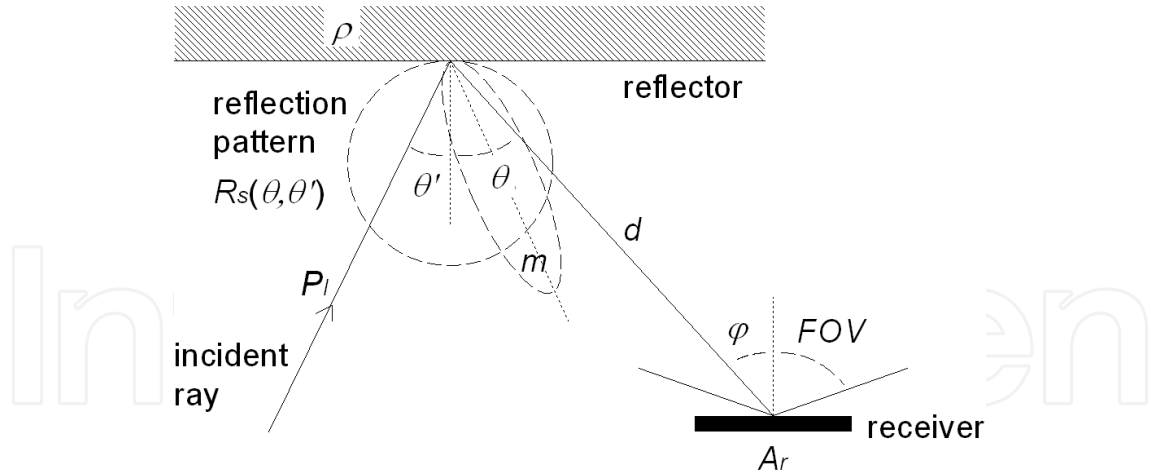


**Figure 2.** Geometry of emitter and receiver with reflectors. Reflection pattern of the surface is described by Phong’s model

by the reflection coefficient of the surface ( $P_{\text{new ray}} = \rho P_I$ ), and the reflected power reaching the receiver is computed by:

$$P_R = \frac{1}{d^2} R_S(\theta, \theta') A_{\text{eff}}(\varphi) \tag{7}$$

where  $d$  is the distance between the reflection point and receiver, and  $R_S(\theta, \theta')$  is Phong’s model, used to describe the reflection pattern of the surface [21]. This model is able to approximate the behaviour of those surfaces that present a strong specular component. It considers the reflection pattern as a sum of both diffuse and specular components. In this way, surface characteristics are defined by two new parameters, the percentage of incident signal that is reflected diffusely  $r_d$  and the directivity of the specular component of the reflection  $m$ . This model is described by:

$$R_S(\theta, \theta') = \rho P_I \left[ r_d \frac{\cos \theta}{\pi} + (1 - r_d) \frac{m + 1}{2\pi} \cos^m(\theta - \theta') \right] \tag{8}$$

where  $\rho$  is the surface reflection coefficient,  $P_I$  represents the optical power of the incident ray,  $\theta$  is the observation angle, and  $\theta'$  represents the incidence angle (see Fig. 2).

### 2.3. The MIMO optical channel

In a typical multi-user application, several emitters can be placed in the room and an *angle-diversity* receiver, composed of multiple receiving elements oriented in different directions, could be used. By using (7), the contribution of the  $i^{\text{th}}$  ray emitted by the  $l^{\text{th}}$  user to the received power reaching each  $j^{\text{th}}$  branch of the receiver during a certain time interval ( $p_{j,i,k}^{(l)}$ ,  $k^{\text{th}}$  time interval) can be computed. The total received power at the  $j^{\text{th}}$  branch of the optical detector in the  $k^{\text{th}}$  time interval (width  $\Delta t$ ) is computed as the sum of the power of the  $N_{j,k}^{(l)}$  rays that contribute in that interval:

$$p_{j,k}^{(l)} = \sum_{i=1}^{N_{j,k}^{(l)}} p_{j,i,k}^{(l)} \tag{9}$$

If we consider a normalized receiver responsivity of 1 A/W, the impulse responses  $h_j^{(l)}(t)$  at all branches ( $j = 1, \dots, P$ ) due to the  $l^{\text{th}}$  user ( $l = 1, \dots, L$ ) are given by:

$$h_j^{(l)}(t) = \sum_{k=0}^{K-1} p_{j,k}^{(l)} \delta(t - k\Delta t) \tag{10}$$

where  $K = t_{\text{max}}/\Delta t$ , and where we have assumed as the time origin the instant when the rays are generated from the emitter. This process must be repeated in order to obtain the different impulse responses between each emitter and each receiving branch in the multi-user scenario.

**Transmitters structure**

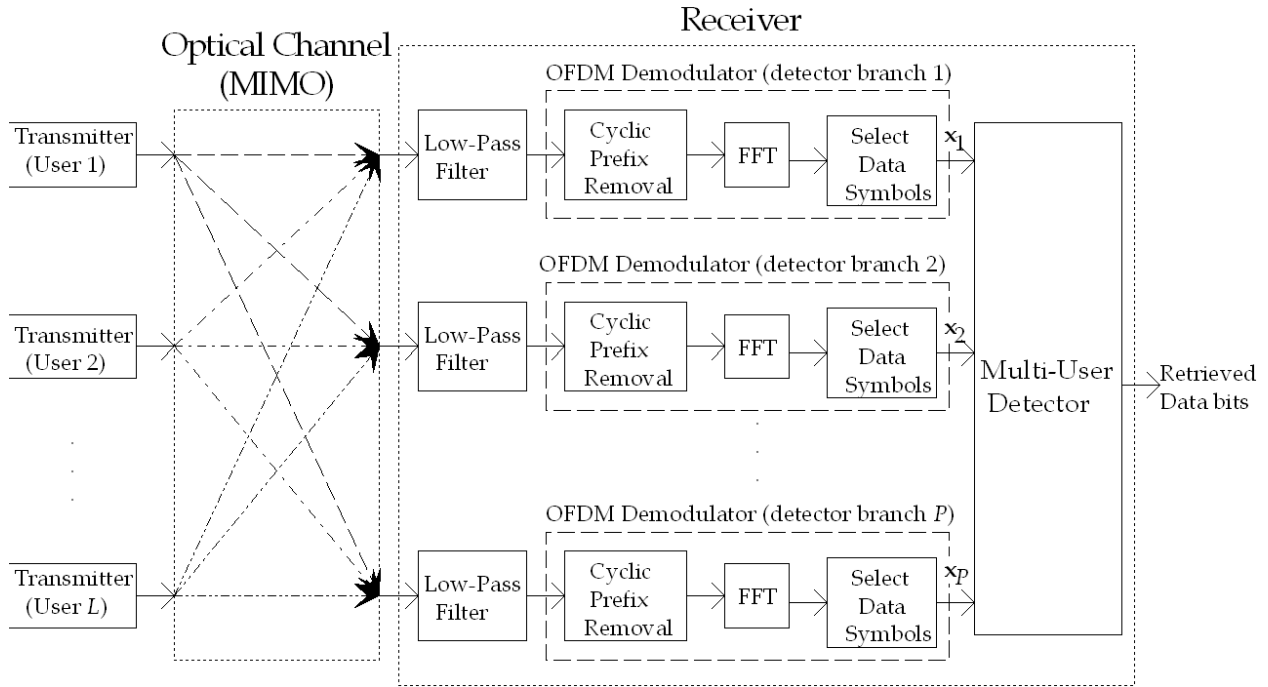
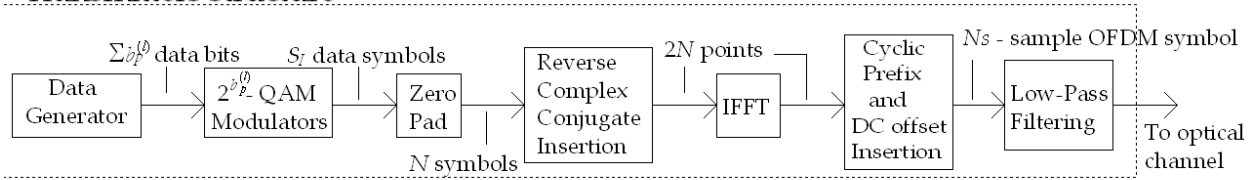


**Figure 3.** Multi-user MIMO-OFDM system for optical wireless communications

**3. The MIMO-OFDM system**

Fig. 3 shows the block diagram of the MIMO-OFDM system for multi-user communications over an indoor wireless optical channel. As we can see in the transmitter structure,  $\sum_p b_p^{(l)}$  data bits are generated by  $l^{\text{th}}$  user and modulated by using an appropriate  $2^{b_p^{(l)}}$ -QAM (quadrature amplitude modulation) modulator,  $b_p^{(l)}$  being the number of bits conveyed by the  $p^{\text{th}}$  subcarrier ( $1 \leq p \leq S_l$ ). In general, we will assume  $b_p^{(l)} = B$  for every subcarrier  $p$  and user  $l$ , but we could accommodate different number of bits to each subcarrier and

user, adapting the throughput to the frequency characteristics of the channel [9]. Then,  $N - S_I$  zeros are padded to this set of  $S_I$  symbols generated by the modulators, the first zero being added before, corresponding to the direct-current (DC) value, and the remaining ones after. Finally, the complex conjugate of the mirror of the word of  $N$  symbols is added before computing the IFFT. The outgoing IFFT symbol is a real sequence of  $2N$  points, which can be made non-negative by adding an appropriate DC level. Moreover, a cyclic prefix ( $N_e$ -sample extension) is inserted to combat ISI, leading to a transmitted signal with a total of  $N_S = 2N + N_e$  samples and duration  $T_S$ . This positive and real signal can modulate the intensity of light emitted by the optical source. Note that the cyclic extension prefix will be ISI-corrupted due to the low-pass channel response and will be discarded at receiver. Next, the FFT of the remaining  $2N$  points will be computed at each receiving branch, and only the first  $S_I$  points (after the DC value) will be considered by the multi-user (MU) detector.

As we have  $L$  transmitters and the receiver possesses  $P$  receiving branches, the optical channel constitutes a MIMO system, whose individual impulse responses are given by (10). We can consider that, after the FFT processing carried out by each branch of a new received OFDM symbol, the  $P$ -branch detector array provides the MU detector with a vector of complex symbols  $\mathbf{x}_p$  at  $p^{\text{th}}$  subcarrier, which is the superposition of the independently distorted signals associated with the  $L$  users sharing the same space-frequency resource and also corrupted by noise at the detector array elements:

$$\mathbf{x}_p = \mathbf{H}_p \mathbf{s}_p + \mathbf{n}_p \quad (11)$$

where the vector  $\mathbf{x}_p \in \mathbb{C}^{P \times 1}$  of received signals at the  $p^{\text{th}}$  subcarrier, the vector  $\mathbf{s}_p \in \mathbb{C}^{L \times 1}$  of transmitted signals and the array noise vector  $\mathbf{n}_p \in \mathbb{C}^{P \times 1}$ , respectively, are given by:

$$\begin{aligned} \mathbf{x}_p &= (x_{1p}, x_{2p}, \dots, x_{Pp})^T \\ \mathbf{s}_p &= (s_p^{(1)}, s_p^{(2)}, \dots, s_p^{(L)})^T \\ \mathbf{n}_p &= (n_{1p}, n_{2p}, \dots, n_{Pp})^T \end{aligned} \quad (12)$$

where  $(\ )^T$  means the transpose of  $(\ )$ , then  $\mathbf{x}_p$ ,  $\mathbf{s}_p$  and  $\mathbf{n}_p$  are all column vectors. The frequency domain channel transfer function factor matrix  $\mathbf{H}_p \in \mathbb{C}^{P \times L}$  is composed of the set of channel transfer vectors  $\mathbf{H}_p^{(l)} \in \mathbb{C}^{P \times 1}$ ,  $l = 1, \dots, L$  of the  $L$  users:

$$\mathbf{H}_p = (\mathbf{H}_p^{(1)}, \mathbf{H}_p^{(2)}, \dots, \mathbf{H}_p^{(L)}) \quad (13)$$

each of which hosts the frequency domain channel transfer factor between the single emitter source associated with a particular user  $l$  and the receiving branches  $j = 1, \dots, P$  at the  $p^{\text{th}}$  subcarrier band:

$$\mathbf{H}_p^{(l)} = (H_{1p}^{(l)}, H_{2p}^{(l)}, \dots, H_{Pp}^{(l)})^T \quad (14)$$

with  $l = 1, \dots, L$ . Note that the frequency domain channel transfer factors  $H_{jp}^{(l)}, \forall p$  between the  $l^{\text{th}}$  emitter and the  $j^{\text{th}}$  receiving branch are obtained by computing the Fourier transform (1) at the subcarrier frequency  $f = pf_0$  over the corresponding impulse response (10), where  $f_0 = 1/T$ . Here,  $T$  is the time duration of the part of the OFDM symbol which actually conveys information, i.e. the OFDM symbol duration excluding the cyclic prefix extension,  $T = 2NT_S / N_S = 2NT_S / (2N + N_e)$ .

### 3.1. Optimum multi-user detection

The optimum detector, when a *maximum a posteriori probability* (MAP) criterion is considered and all the symbols are assumed, *a priori*, to have equal probability of being transmitted, is the *maximum likelihood* (ML) detector [26]. This detector finds the specific  $L$ -dimensional vector of  $M$ -ary symbols ( $M = 2^B$ ), which is more likely to have been transmitted. In formal terms, ML detection is based on the idea of maximising the *a posteriori* probability  $P(\check{\mathbf{s}}_p | \mathbf{x}_p, \mathbf{H}_p)$  that a specific vector  $\check{\mathbf{s}}_p \in \mathbb{C}^{L \times 1}$  of the different users' symbols was transmitted over the MIMO channel characterised by the channel transfer factor matrix  $\mathbf{H}_p \in \mathbb{C}^{P \times L}$  under the condition that the vector  $\mathbf{x}_p \in \mathbb{C}^{P \times 1}$  was received at the MU detector end. Note that each evaluated vector  $\check{\mathbf{s}}_p$  is an element of a set  $\mathcal{M}_p^L$  with a total of  $M^L$  possible trial-vectors. The aforementioned maximisation can be expressed as:

$$\check{\mathbf{s}}_{p,\text{ML}} = \arg \max_{\check{\mathbf{s}}_p \in \mathcal{M}_p^L} P(\check{\mathbf{s}}_p | \mathbf{x}_p, \mathbf{H}_p) \quad (15)$$

For the optical AWGN channel, maximising  $P(\check{\mathbf{s}}_p | \mathbf{x}_p, \mathbf{H}_p)$  is equivalent to minimising the Euclidean distance metric  $\|\mathbf{x}_p - \mathbf{H}_p \check{\mathbf{s}}_p\|_2^2$ ,  $\forall \check{\mathbf{s}}_p \in \mathcal{M}_p^L$  [12], and hence we have:

$$\check{\mathbf{s}}_{p,\text{ML}} = \arg \max_{\check{\mathbf{s}}_p \in \mathcal{M}_p^L} P(\check{\mathbf{s}}_p | \mathbf{x}_p, \mathbf{H}_p) \Leftrightarrow \check{\mathbf{s}}_{p,\text{ML}} = \arg \min_{\check{\mathbf{s}}_p \in \mathcal{M}_p^L} \|\mathbf{x}_p - \mathbf{H}_p \check{\mathbf{s}}_p\|_2^2 \quad (16)$$

where  $\|\cdot\|_2^2$  denotes the squared Euclidean norm. The ML detection is excessively costly for typical values of  $M$ -ary modulation and number of transmitting users  $L$ , since the receiver must evaluate a total of  $M^L$  Euclidean distance calculations (16) for each  $p^{\text{th}}$  subcarrier, with  $S_I$  being the total number of subcarriers. For example, for 16-QAM modulation and  $L = 3$  users, the total number of operations by each subcarrier is 4096, which is impractical. Therefore, sub-optimum detection techniques have been devised in order to reduce the dimensionality of the classification problem associated with selecting the specific constellation point, which is most likely to have been transmitted by each user. Linear detection techniques are based on obtaining linear estimates of the different users' transmitted signals with the aid of the weighted combining of the signals received by the different detector elements. This is followed by separately demodulating each of the  $L$  different users' combiner output signals. Thus, the original  $M^L$ -dimensional classification problem associated with the optimum ML detection is reduced to  $L$  individual classification steps, each having a dimensionality of  $M$ . In fact, the corresponding receiver associated with the  $l^{\text{th}}$  transmitting user only has to carry out one of these  $L$  classifications to retrieve the data that concerns it. However, when using optimal ML detection, the receiver has to carry out  $M^L$  evaluations of (16) in spite of being concerned with only the data transmitted by its corresponding  $l^{\text{th}}$  user.

### 3.2. Least squares error detector

Using a linear detector, an estimate  $\hat{\mathbf{s}}_p \in \mathbb{C}^{L \times 1}$  at the  $p^{\text{th}}$  subcarrier band of the vector of transmitted signals  $\mathbf{s}_p$  of the  $L$  simultaneous users is generated by linear combining the signals received by the  $P$  different receiving branches with the aid of a weight matrix  $\mathbf{W}_p \in \mathbb{C}^{P \times L}$ :

$$\hat{\mathbf{s}}_p = \mathbf{W}_p^H \mathbf{x}_p \quad (17)$$

where  $\mathbf{W}_p^H$  denotes the complex conjugate matrix of the matrix  $\mathbf{W}_p$ . When least-squares (LS) error detector is considered, also called zero-forcing (ZF) combiner, the weight matrix  $\mathbf{W}_{p,LS} \in \mathbb{C}^{P \times L}$  is given by [12]:

$$\mathbf{W}_{p,LS} = \mathbf{H}_p \left( \mathbf{H}_p^H \mathbf{H}_p \right)^{-1} \quad (18)$$

By substituting the received signal's model of (11) and the LS estimation based weight matrix (18) into (17), we obtain:

$$\hat{\mathbf{s}}_{p,LS} = \mathbf{s}_p + \mathbf{W}_{p,LS}^H \mathbf{n}_p \quad (19)$$

which indicates that the LS-estimate  $\hat{\mathbf{s}}_{p,LS}$  of the transmitted signal vector  $\mathbf{s}_p$  of the  $L$  simultaneous users is an unbiased noise-contaminated version of  $\mathbf{s}_p$ , so that  $E \{ \hat{\mathbf{s}}_{p,LS} \} = \mathbf{s}_p$ . When using the LS combiner, the  $l^{\text{th}}$  user's associated vector component of estimate (17) of the vector of transmitted signals at the  $p^{\text{th}}$  subcarrier can be expressed as:

$$\hat{s}_{p,LS}^{(l)} = \mathbf{W}_{p,LS}^{(l)H} \mathbf{x}_p \quad (20)$$

where the  $l^{\text{th}}$  user's associated weight vector  $\mathbf{W}_{p,LS}^{(l)} \in \mathbb{C}^{P \times 1}$  coincides with the  $l^{\text{th}}$  column vector of the matrix  $\mathbf{W}_{p,LS}$ . The complex symbol that is most likely to have been transmitted by the  $l^{\text{th}}$  user can be determined upon minimising the Euclidean distance between estimate (20) of the transmitted signal obtained at the  $l^{\text{th}}$  user's combiner output and all the constellation points associated with the specific modulation scheme employed. This only requires  $M$  evaluations as compared to the  $M^L$  ones of the optimum ML detector.

### 3.3. Frequency-domain channel transfer factor matrix estimation

From (18) and (20), we can observe that the LS detector requires the knowledge of the transfer factor matrix  $\mathbf{H}_p$ . The method described in [8], where TS known training sequences are used to estimate the channel transfer function between a single user and the receiver, can be used to estimate the matrix  $\mathbf{H}_p$ , assuming that only one user is transmitting in a specific instant during the training periods. If a certain known training sequence  $X_p$  is transmitted by the  $l^{\text{th}}$  user over the slowly time-varying wireless optical channel, the channel response of each sub-band  $H_{jp}^{(l)}$  for this user at the  $j^{\text{th}}$  receiving branch can be estimated from the  $S_I$  received symbols ( $Y_{jp}^{(l)}$ ) as follows:

$$\hat{H}_{jp}^{(l)} = Y_{jp}^{(l)} / X_p \quad (21)$$

Note that the  $\hat{H}_{jp}^{(l)}$  values are distorted by noise and therefore several training sequences should be transmitted, and then the mean values of the estimates can be used to obtain a better channel characterisation. In fact, by using ten training sequences, the channel response estimation given by (21) is very close to the actual channel response, and we will obtain a system performance very similar to that of the ideal case when a perfect knowledge of the channel response is available [8].

## 4. Simulation results

In this section, the previously described multi-user OFDM system is evaluated by means of simulations with a maximum number of  $L = 6$  simultaneous users. The simulated room

is 7.5 m long  $\times$  5.5 m wide  $\times$  3.5 m high [5] (see Table 1 for additional information about the room's characteristics and other simulation parameters: the north wall is the first you come across if you enter the room along the  $x$ -direction). The emitters are attached to the ceiling at different positions and their main lobes are pointed straight down (see Fig. 4). The emitters have three lobes of radiation modelled as second order Lambertian (half-power beam width, HPBW =  $45^\circ$ ): their side lobes are titled at  $45^\circ$  pointing in opposite directions with respect to the ceiling normal and one of them points towards the centre of the room floor, where the receiver is located. The receiver consists of  $P = 6$  branches of equal field of view (FOV),  $\phi_b = 40^\circ$ . The central branch is oriented towards the ceiling, whereas the five side branches are tilted at  $45^\circ$  and distributed uniformly at  $72^\circ$  in azimuth, as depicted in Fig. 4. Table 2 summarises the main characteristics of emitters and receiver (in the table,  $\gamma_i$  is the angle subtended between the  $x$ -axis and an imaginary line drawn from the position of the  $i^{\text{th}}$  emitter towards the centre of the ceiling).

Room parameters	
length ( $x$ ):	7.5 m
width ( $y$ ):	5.5 m
height ( $z$ ):	3.5 m
$\rho_{NORTH}$ :	0.30
$\rho_{SOUTH}$ :	0.56
$\rho_{EAST}$ :	0.30
$\rho_{WEST}$ :	0.12
$\rho_{CEILING}$ :	0.69
$\rho_{FLOOR}$ :	0.09
Simulation parameters	
Number of rays ( $N$ ):	1 000 000
Number of maximum reflections ( $K$ ):	20
Resolution ( $\Delta t$ ):	0.2 ns
Simulation time ( $t_{\max}$ ):	100 ns

**Table 1.** Parameters for simulation

Emitters Locations: ( $x y z$ ) m	Radiation pattern	Receiver
Emitter 1: (0.75 0.75 3.5)	Mode( $n$ ): 2	Position ( $x y z$ ) m: (3.75 2.75 0.75)
Emitter 2: (6.75 0.75 3.5)	Number of radiation lobes: 3	Area: $1 \text{ cm}^2$
Emitter 3: (3.75 2.75 3.5)	Orientation (elevation, azimuth):	FOV: $40^\circ$
Emitter 4: (0.75 4.75 3.5)	( $135^\circ \gamma_i$ ), ( $180^\circ 0^\circ$ ),	Orientation of detector branches (elevation, azimuth):
Emitter 5: (3.75 4.75 3.5)	( $135^\circ \gamma_i + 180^\circ$ )	( $0^\circ 0^\circ$ ), ( $45^\circ 0^\circ$ ), ( $45^\circ 72^\circ$ )
Emitter 6: (6.75 4.75 3.5)		( $45^\circ 144^\circ$ ), ( $45^\circ 216^\circ$ ), ( $45^\circ 288^\circ$ )

**Table 2.** Parameters of emitters and receiver

The channel impulse responses from each emitter (user) to each receiving branch have been computed by using the modified Monte Carlo based ray-tracing algorithm described in section 2. We can easily anticipate that the impulse responses of the main channel between a certain user and the receiver will have a predominant LOS contribution because there is always at least one branch of the receiver directly observing every point on the ceiling (see observed impulses responses at each receiving branch in Fig. 5). This configuration could be considered as not sufficiently exploiting the angle-diversity provided by the receiver and

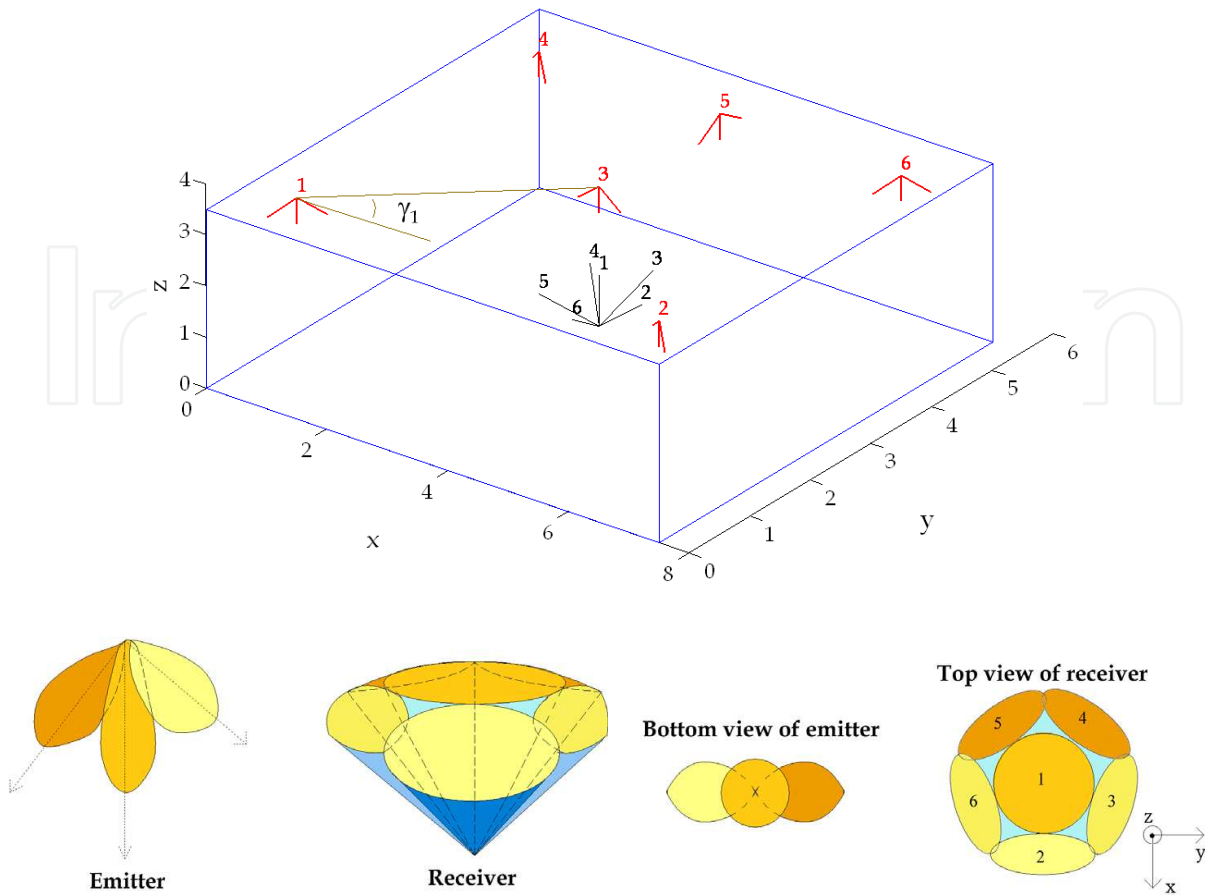


**Figure 4.** Location and structure of the six transmitters and the receiver in the simulation room

that non-LOS links should also be taken into account. However, the combination of the angle-diversity receiver with the MU detector enables multi-user communication whenever the emitters are moved apart, so the receiver does not see them as quasi-identical light sources. In addition, the LS combiner also requires that the maximum number  $L$  of simultaneous users does not outweigh the number  $P$  of receiving branches [12]. Therefore, we have considered LOS links as a more realistic situation, especially for a potential system based on visible LED lighting (VLC: *Visible Light Communications*). The main advantage of LOS links is the remarkably lower transmission power required to obtain the same performance as their non-LOS counterparts. However, it is vulnerable to shadowing: the LOS link can be blocked momentarily by the presence of an obstacle or a human between emitter and receiver. This can be solved by using redundant emitters or providing the system with more directive emitters (larger lobe order  $n$ ) and receivers (narrower FOVs) where shorter quasi-vertical links prevail over longer distance smaller-angle horizontally-tilted ones, which are prone to blocking. The shorter quasi-vertical links allow us to establish different communication networks inside a room as their high directivity avoids interferences with neighbouring zones beyond a few metres. This is the underlying idea in VLC, where illumination lamps are used to enable transmission mainly with the receiving devices just underneath them. However, despite having chosen to evaluate LOS links in this chapter as a more convenient study of future applications, the results presented here can be easily extrapolated to non-LOS configurations. The only difference is that, in the latter, the emissions from one user usually affect several branches (three or more) at the receiver, which demands a greater “effort” from the MU detector to “separate” the different signals received. Hence, a greater signal-to-noise ratio

(SNR) will be required, as compared to the LOS counterparts, to obtain a certain level of performance. Moreover, we must not forget that greater transmission powers are also needed to reach those required SNR values. Typical non-LOS configurations would require up to ten decibels more in the SNR at the receiver than LOS links [9], which would make them impractical in many applications.

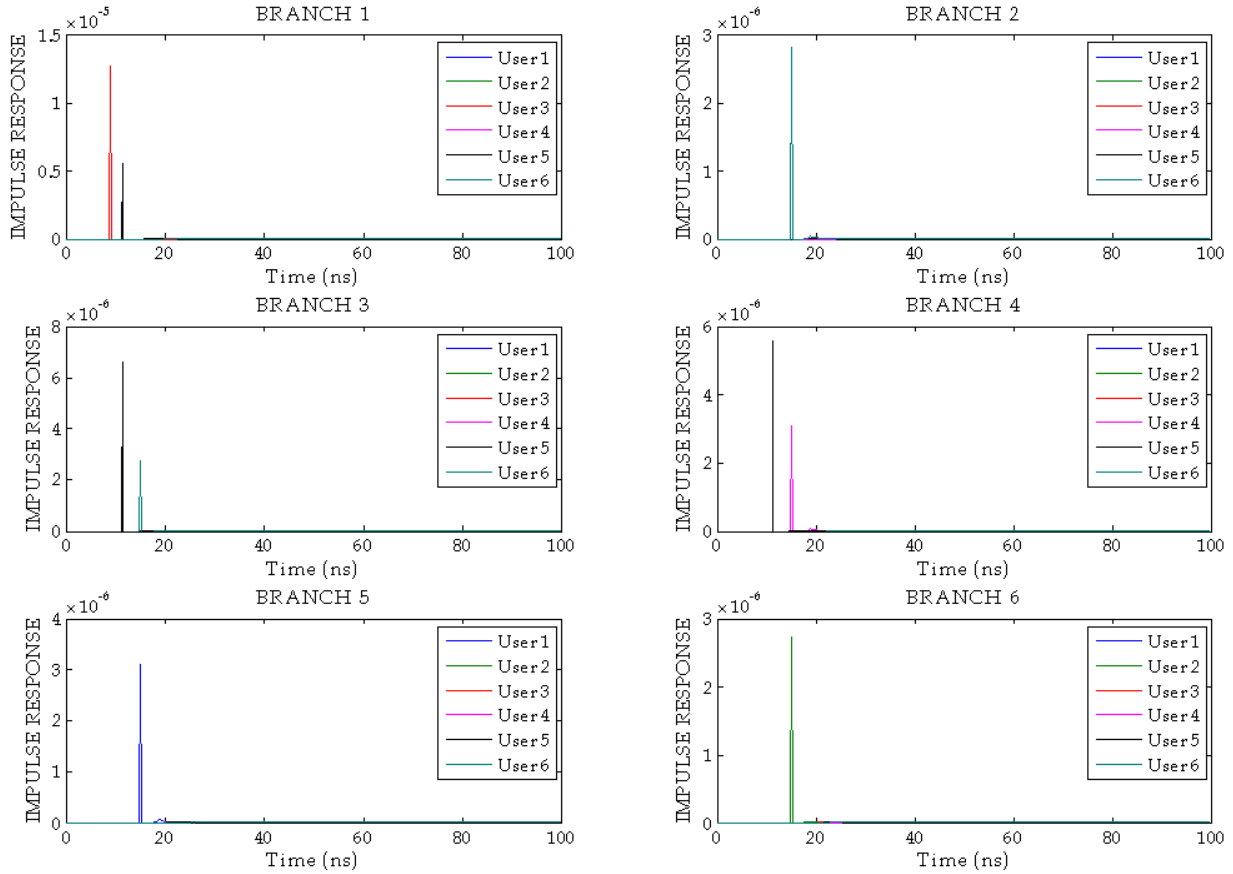


**Figure 5.** Impulses responses between the transmitting users and each receiving branch

In all the simulation results presented below, the number of subcarriers is  $N = 64$  (128-point FFT), but only  $S_I = 52$  convey data ( $2^B$ -QAM modulated). A cyclic prefix extension of  $N_e = 32$  samples was used and the transmission symbol rate was 1 Msymbol/s, which leads to a total system throughput of  $B \times S_I \times L$  Mbit/s (e.g. 1.248 Gbit/s for  $L = 6$  users with every subcarrier 16-QAM modulated). This OFDM symbol extension ( $N_e / (2N + N_e) = 200$  ns) is large enough to compensate for ISI in most of the non-LOS diffuse links scenarios, hence its length could be reduced up to four times if only LOS configurations are considered (in this case, the efficiency of the OFDM transmission  $2N / (2N + N_e)$  would increase from 80% to roughly 95%). However, here we have considered a more general system, valid for practically any kind of optical link. In this case, the separation between subcarriers is  $\Delta f = f_0 = 1.25$  MHz, leading to a transmission bandwidth of approximately  $B_T = S_I \Delta f = 65$  MHz plus a convenient out-of-band guard [8], which is extremely practical for typical optical devices. Finally, we used ten training sequences to estimate (using the method described in section 3.3) the frequency-domain channel transfer function factors of matrix  $\mathbf{H}_p$  required by LS detector to obtain the weight matrix (18) or for evaluating (16) in the case of ML detector.

### 4.1. Comparison of maximum-likelihood and least-squares detection

In this subsection, the bit error rate (BER) performance of the multi-user detector based on the maximum-likelihood criterion is compared with that of least-squares error detector for  $L = 3$  simultaneous users. Fig. 6 shows the BER performance as a function of the number  $B$  of transmitted bits per subcarrier (BPSK, QPSK and 16-QAM are considered). For reference purposes, the figure also depicts the results for the case of single-user transmission ( $L = 1$ ) in contrast to those of the multi-user ( $L = 3$ ) scenario. As mentioned in subsection 3.1, ML detection would require  $2^{BL} = 4096$  classifications for each subcarrier when 16-QAM is considered for  $L = 3$  users or when addressing QPSK for  $L = 6$  users, both situations being impractical in a real application. Therefore, we are not able to assess the  $L_{\max} = P = 6$  users scenario in this comparison because it would require  $2^{4 \times 6} = 16777216$  classifications per subcarrier for 16-QAM, a prohibitive number even in a simulation. Thus, the results shown have been obtained for the fifth user of the communication scenario illustrated in Fig. 4 when users 4 and 6 are also transmitting. This constitutes one of the worst-case situations, since emissions from user 5 are strongly interfered at receiving branches 1, 3 and 4 by other users (see Fig. 5), especially by users 1, 4 and 6.

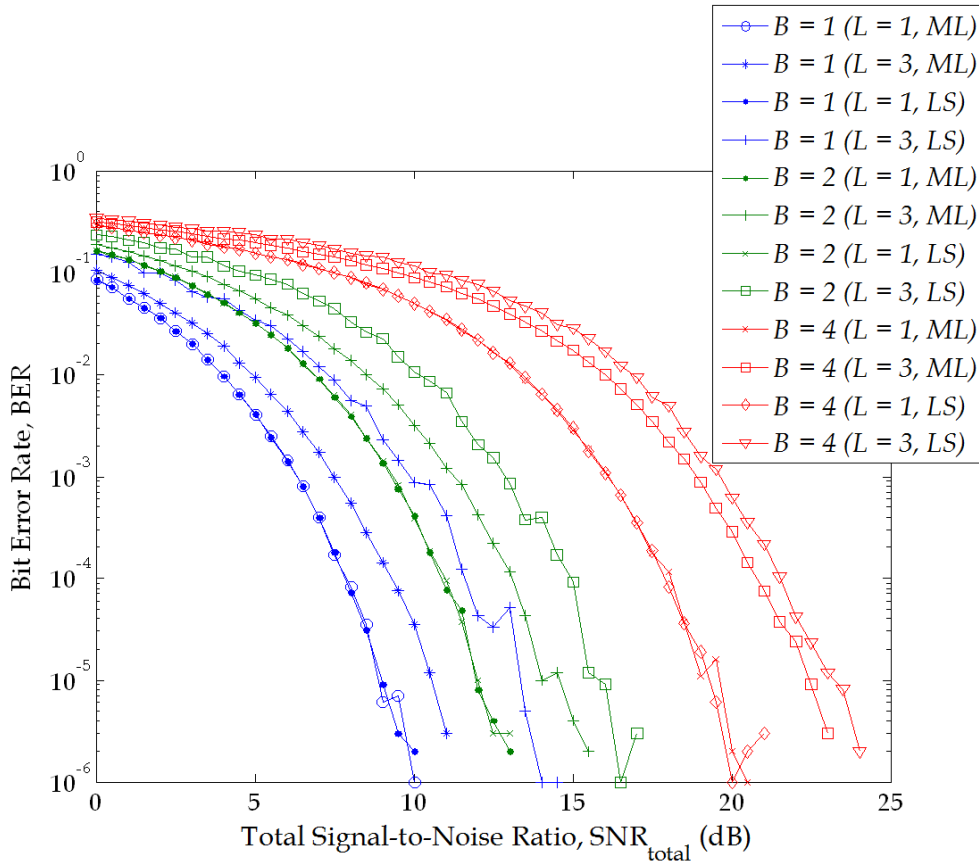


**Figure 6.** Performance comparison of ML and LS detection for the fifth user (worst case) when the subcarriers are  $2^B$ -QAM modulated

For the single-user scenario,  $\mathbf{H}_p \in \mathbb{C}^{P \times 1}$  is a column-vector which leads to the LS estimation based weight matrix  $\mathbf{W}_{p,LS}$  being reduced to:

$$\mathbf{W}_{p,LS}^{(L=1)} = \mathbf{H}_p \left( \mathbf{H}_p^H \mathbf{H}_p \right)^{-1} = \frac{\mathbf{H}_p}{\mathbf{H}_p^H \mathbf{H}_p} = \frac{\mathbf{H}_p}{\|\mathbf{H}_p\|^2} \tag{22}$$

where  $\|\mathbf{H}_p\|^2 = H_{1p}^H H_{1p} + H_{2p}^H H_{2p} + \dots + H_{Pp}^H H_{Pp}$  is a real number. Therefore, for the single-user case, the estimation of the transmitted symbol  $s_p$  at the  $p^{\text{th}}$  subcarrier given by (17) yields:

$$\hat{s}_p^{(L=1)} = \mathbf{W}_{p,LS}^{(L=1)H} \mathbf{x}_p = \frac{\mathbf{H}_p^H \mathbf{x}_p}{\|\mathbf{H}_p\|^2} \quad (23)$$

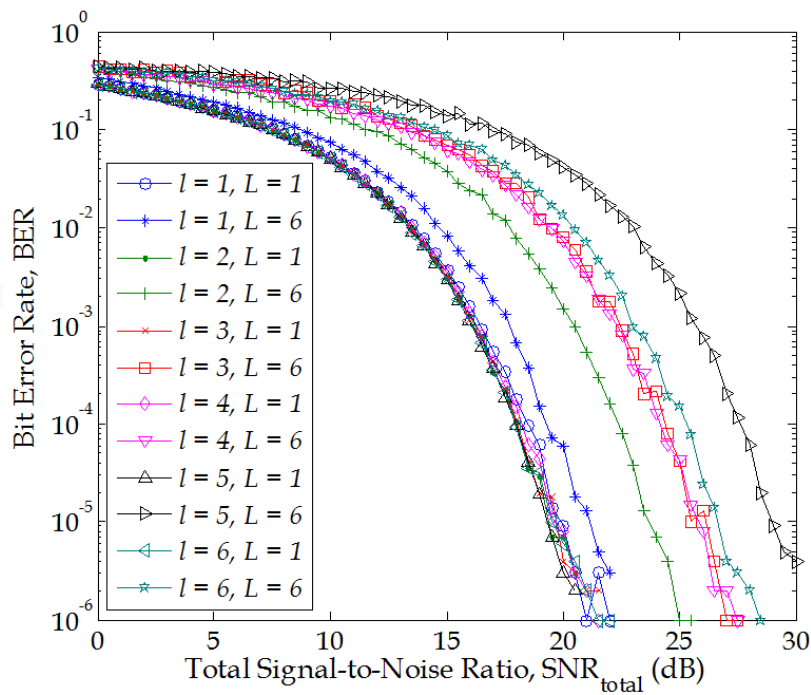
Minimising the Euclidean distance between the previous estimate  $\hat{s}_p^{(L=1)}$  and all the constellation points associated with the specific modulation scheme employed is equivalent to the evaluation of (16) carried out by the ML detector. Hence, both ML and LS methods perform equally and optimally in the single-user scenario. This is why we can observe identical results for a given  $2^B - \text{QAM}$  modulation scheme in the  $L = 1$  cases irrespective of the detection method used. However, when receivers deal with a multi-user scenario, the ML detector outperforms the LS-based one by several decibels. Nonetheless, the greater the modulation scheme employed, the smaller the SNR gain obtained by the optimum receiver with respect to that of the suboptimal LS detector. Thus, we can see how SNR gains of about 3 dB for BPSK are reduced to less than 1 dB when 16-QAM is considered. In addition, taking into account that the LS detector only requires 4 and 16 classifications associated with a specific user for QPSK and 16-QAM, respectively, in contrast to the 64 and 4096 needed by the ML detector for  $L = 3$  users, we can conclude that the simplicity and fairly close to optimum performance of LS detection makes it a practical and better choice for multi-user communication scenarios.

## 4.2. Performance of multi-user LS detector

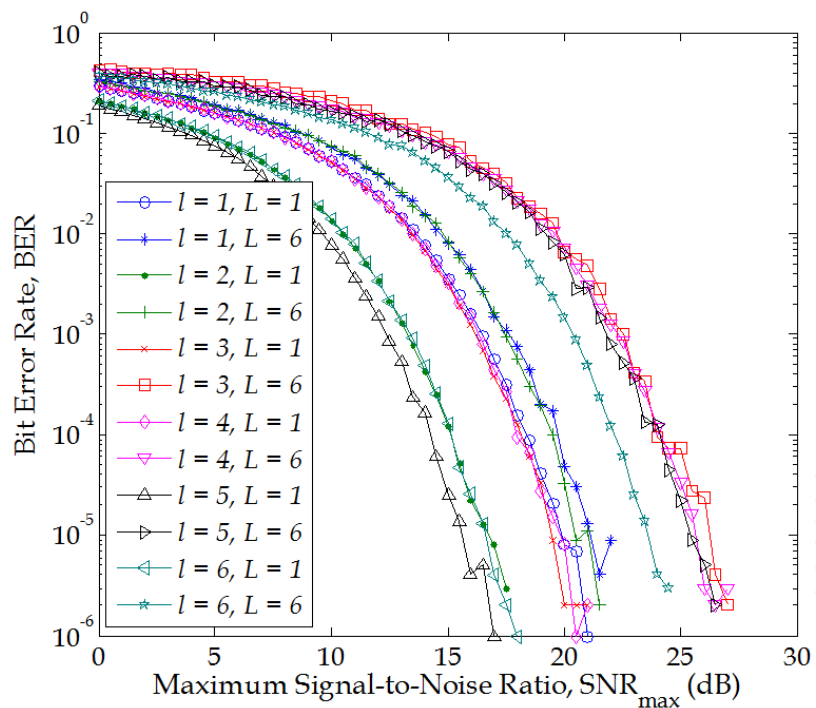
Fig. 7 draws together the simulation results obtained for each  $l^{\text{th}}$  user depicted in Fig. 4 for two situations: when only the desirable user is transmitting (ideal case, specified as  $L = 1$  in the legend) and for the full-user scenario, i.e. when all the  $L = L_{\text{max}} = 6$  users are transmitting simultaneously.

In Fig. 7(a), the BER is depicted versus the total signal-to-noise ratio, the latter obtained as  $\sum_{j=1}^P \text{SNR}_j^{(l)}$  ( $\text{SNR}_j^{(l)}$  is the SNR at  $j^{\text{th}}$  receiving branch for the  $l^{\text{th}}$  user). It can be seen how all the users present the same performance under the single-user scenario, which coincides with that of 16-QAM OFDM systems over ideal additive white Gaussian noise (AWGN) channels [8]. We can also observe how the fifth user ( $l = 5$ ) performs the worst under the multi-user ( $L = 6$ ) scenario, requiring about ten decibels more than the single-user case. In contrast, the first user ( $l = 1$ ) presents a SNR loss of hardly 1 dB between multi-user and single-user scenarios. The previous results are logical, since the fifth user is located in the worst position of the room, sharing several receiving branches at the detector with other users as we mentioned previously, whereas the first emitter is alone in a corner and the only one that illuminates the fifth receiving branch of the detector (see Fig. 4 and 5).

Despite Fig. 7(a) showing a performance loss of the multi-user system with respect to the single-user scenario, it does not allow us to discover the required SNR at each branch to obtain the observed performance. Fig. 7(b) shows the same results as before, but representing the BER versus the maximum SNR at the receiver for the  $l^{\text{th}}$  user, i.e.  $\max(\text{SNR}_j^{(l)}), j = 1, \dots, P$ . In this graph, we can see how users  $l = 3, 4$  and  $5$  present a very similar performance when facing the multi-user scenario, i.e. all of them require approximately the same SNR at the branch which receives the most light power from the corresponding user in order to obtain a given



(a) BER vs. Total SNR



(b) BER vs. Maximum SNR

**Figure 7.** BER vs. total and maximum SNR for each  $l^{\text{th}}$  user when all the subcarriers are 16-QAM modulated

BER. That is, they require similar “effective” emission powers to obtain a certain performance. However, user 5 directly illuminates three branches ( $j = 1, 3$  and  $4$ , see Fig. 5), although the electrical power of the induced-photocurrent at the third receiving branch practically doubles

those at the other two branches. To the contrary, users 3 and 4 only directly illuminate one branch, the first and fourth, respectively, the received power at the remaining branches being negligible. Therefore, given a similar “effective” emitted power, the total electrical power at the detector due to user 5 is approximately twice that due to users 3 and 4, leading to the different performances observed in Fig. 7(a) of approximately 3 dB (actually, slightly more) worse for user 5. Additionally, with this new representation criterion, the loss in dB between the multi-user and single-user scenario performances remains unchanged for each user (with respect to that observed in Fig. 7(a)), as expected. However, single-user performances are not all identical as before: the users that directly illuminate more than one branch improve by three or more dB their single-user performance, with respect to those which only illuminate one branch directly. Finally, users 1 and 2 present the best multi-user performances.

Therefore, we can conclude that Fig. 7(b) offers a better performance comparison than Fig. 7(a), since it shows us the true SNR required at receiver branches to obtain a specific BER, regardless of how many branches are simultaneously illuminated by each user.

### 4.3. Complexity reduction of least-squares detector

The main limitation of linear multi-user detectors is the fact that a weight matrix  $\mathbf{W}_p$ ,  $\forall p$  has to be determined. For the simplest LS detector, obtaining each of these weight matrices involves, according to (18), multiplying two complex matrices ( $\mathbb{C}^{L \times P}$  and  $\mathbb{C}^{P \times L}$ , respectively), the inversion of the resulting  $\mathbb{C}^{L \times L}$  matrix and a final  $\mathbb{C}^{P \times L} \times \mathbb{C}^{L \times L}$  multiplication. However, this very complicated operation only has to be carried out once after a specific training period has provided new estimates of the frequency-domain channel transfer factor matrices  $\mathbf{H}_p$ . For slowly time-varying wireless optical channel, this operation could occur with a very low periodicity in time.

In contrast, obtaining the estimates  $\hat{s}_p$  of the different users’ transmitted signals for each subcarrier must be done every OFDM symbol period  $T_S$ . According to (17), this operation requires a  $\mathbb{C}^{L \times P} \times \mathbb{C}^{P \times 1}$  matrix multiplication by each subcarrier. When we are only concerned with the data due to a specific user, operation (20) must be evaluated, which only requires the multiplication of two  $P$ -element complex vectors, i.e.  $P$  complex multiplications and sums by each subcarrier. In any case, the total number of operations can be reduced considerably if we take into account the actual interrelation between users at the receiver, that is, how emissions from other users interfere with that of our desired user. For example, from Fig. 4 and 5, it can be easily observed how the first user is the only one that directly illuminates the fifth branch of the receiver: the received power on it due to the remaining users is negligible. Therefore, demodulating the first user’s data could be carried out by only considering this branch, then turning the evaluation of (20) into a single-user single-branch (SISO, *single-input single-output*) problem:

$$\hat{s}_{p,LS}^{(l=1)} = \mathbf{W}_{p,LS}^{(l=1,j=5)H} \mathbf{x}_p^{(j=5)} = \left( \frac{H_{5p}^{(l=1)}}{H_{5p}^{(l=1)H} H_{5p}^{(l=1)}} \right)^H x_{5p} = \frac{x_{5p}}{H_{5p}^{(l=1)}} \quad (24)$$

Obviously, the multi-user detection problem could be more complex for other users. For example, user 3 only directly illuminates the first branch. But this branch is also illuminated by user 5, which also illuminates branches 3 and 4. However, users 6 and 4, respectively, also illuminate these branches. Therefore, the demodulation of the third user’s data involves considering the received signals at, at least, branches 1, 3 and 4. In this case, the number

of users ( $L = 4$ ) would outweigh the number of branches concerned ( $P = 3$ ). Then, an additional branch must be considered in order to fulfil the condition  $P \geq L$  required by LS detectors. Thus, branch 2 must be chosen, since this is another one illuminated by user 6, in addition to branch 3. However, branch 2 is also affected by emissions from user 2, which additionally illuminates branch 6. Finally, the detection of the data coming from only user 3 requires processing the signals received at all the branches except the fifth.

A simple algorithm can be developed to find the minimum number of branches required for the detection of a certain user's data. Let  $u_j$  be a vector that includes the users' indexes that significantly illuminate the  $j^{\text{th}}$  receiving branch,  $n_j$  the total number of users illuminating that branch, and  $b_l$  a vector that includes the indexes of the branches illuminated by a certain user  $l$ . The algorithm for obtaining the minimum set of branches required to demodulate the data from the  $l^{\text{th}}$  user can be described as follows:

1. Find  $j$  so that minimises  $n_j$ :  $l' \in u_j$
2. Set  $x = j$
3. Set  $x' = x$
4.  $\forall j \in x$ , repeat 5
5.  $\forall l \in u_j$ ,  $x = x \cup b_l$
6. If  $x \neq x'$  go back to 3
7.  $x$  contains the branches to consider for demodulating  $l^{\text{th}}$  user's data

Fig. 8 compares the performance of the original LS detector, which uses all the  $P_{\max} = 6$  branches to demodulate the data corresponding to the different users, and a reduced version of this which only uses the minimum set of  $P_{\min}$  branches obtained by using the previous algorithm. The modulation mode was 16-QAM for every subcarrier. The results have been shown versus the total SNR because they are easier to visualise as compared with maximum SNR results where the greater overlapping of the curves hinders its analysis enormously. However, here we are concerned with comparing BER performance of reduced and original LS detectors for each  $l^{\text{th}}$  user and not comparing the different performances between users. In the graphs, total SNR refers, as in section 4.2, to the sum of the SNRs at each branch for the corresponding user:  $\sum_{j=1}^P \text{SNR}_j^{(l)}$  where  $P = P_{\max} = 6$  irrespective of whether complexity reduction is applied by using fewer branches during demodulation or not. Therefore, reduced and original LS detectors are compared fairly, contrasting their performances with the same total SNR. Surprisingly, we can see how the reduced LS detector outperforms, although with less than 1 dB gain, the original one for all the users (the unique exception being  $l = 2$  for  $\text{SNR}_{\text{total}} > 23$  dB). This can be explained by the fact that, when using all the receiving branches, the residual interference due to the remaining users at each branch impairs the multi-user detector performance, especially when some branches do not receive any signal contribution from the corresponding user. Thus, for example, in the case of the first user, it seems evident that a better performance would be obtained by "switching off" all the receiving branches except the fifth. Therefore, the results show that not only better performance is achieved with the reduced LS detector but also a significant reduction in the complexity of the detection process. Except for users 3 and 4 with slight receiver reductions from 6 to 5 branches, the remaining users can operate perfectly by using only half or fewer of the total receiving branches.

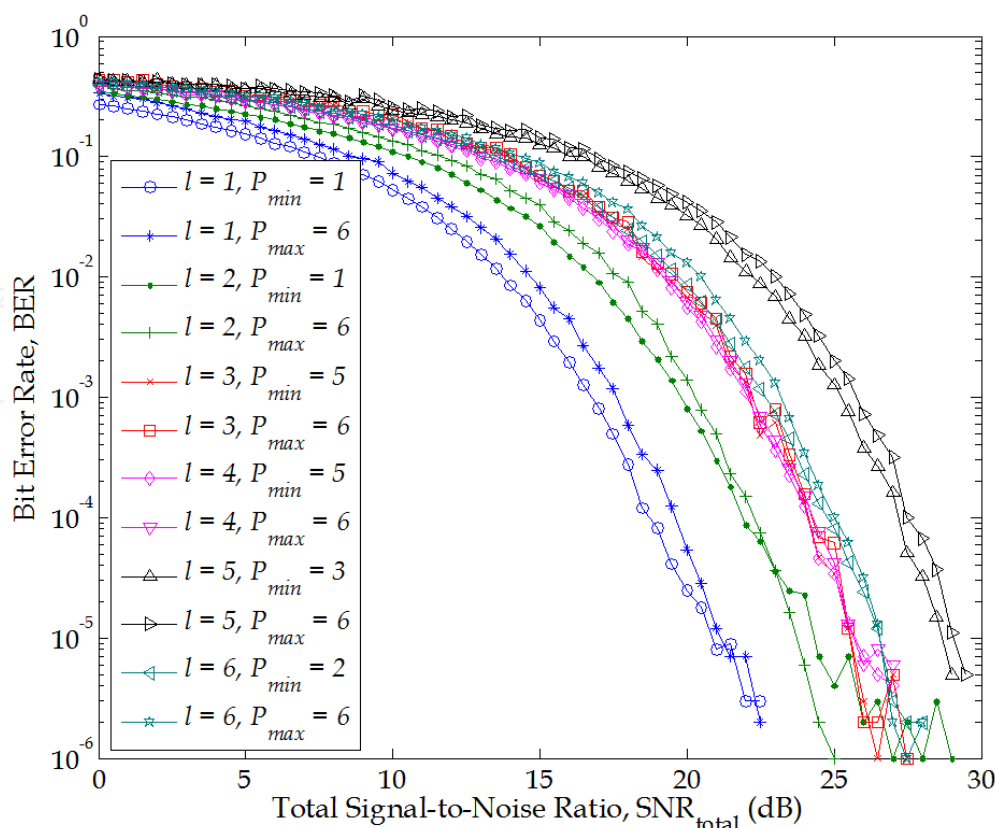


**Figure 8.** Performance comparison of reduced and original LS detectors for each  $l^{\text{th}}$  user when all the subcarriers are 16-QAM modulated

## 5. Other MIMO techniques for WOC

As we have seen, the main limitation of LS-based multi-user detection is its high complexity, since it is implemented on a subcarrier-to-subcarrier basis. This complexity can be reduced significantly as described in section 4.3, without forgetting the beneficial capacity of OFDM for accommodating the system throughput to the channel characteristics and number of simultaneous users [9]. However, despite the complexity of the detection process for a particular user being only proportional to the number  $P$  of receiving branches, obtaining the weight matrix grows exponentially with this number. Therefore, this multi-user technique is only appropriate for scenarios with a reduced number  $L$  of users (since  $P$  must always meet the requirement  $P \geq L$ ).

When we are interested in scenarios with large numbers of users, multi-carrier code-division multiple access (MC-CDMA) is a more practical solution [2]. The lower complexity of MC-CDMA to accommodate larger numbers of users implies a compensation payment. Now, the total throughput provided by the OFDM system is shared among all the simultaneous users. This is accomplished by their corresponding orthogonal codes, which avoid any collision between the user's transmissions at a certain subcarrier in a specific instant in time. That is, never there are two users occupying the same frequency-time resource. This can be compared with the multi-user detection techniques presented in this chapter, where the system takes advantage of the spatial diversity provided by the MIMO channel to separate all the users' signals that are continuously being transmitted using all the available bandwidth.

Outside the OFDM context, there are other multiple works addressing MIMO techniques for indoor wireless optical communications, which are generally applied in conjunction with conventional optical modulation schemes (on-off keying, pulse-position modulation, etc.). The main idea of an important group of them relies on creating many nearly-ideal and independent channels between a specific user and receiver by using multibeam transmitters and angle-diversity receivers [1, 14]. Imaging receivers have also been proposed to greatly increase the number of receiving channels at a reduced cost [6, 16], hence providing higher data rates [3, 29]. Sometimes, the distinctive spatial nature of the channel, which is unique, between a specific transmitter and the receiver is exploited to carry additional information as in optical spatial modulation [22].

## 6. Visible light communications: the new challenge

Visible light communications (VLC), first proposed by researchers at Keio University in Tokyo [18, 19] have prompted the interest of the scientific community in the last few years [7, 11, 17, 25, 29]. There have also been regulatory efforts made on this technology that have led to the appearance of a standard [13]. These new VLC systems, using visible LED lamps to simultaneously transmit information together with their normal use as illumination devices, share the same advantages as their infrared counterparts [15]. They are also eye-safe (visible light is not harmful to the human eye), which enables the use of higher transmission powers. However, the main drawback is the limited transmission bandwidth of current LED devices, typically several MHz, and whose enhancement has been one of the main issues addressed by researchers [23, 24]. Zeng et al. [29] have proposed the use of MIMO schemes based on imaging receivers in order to obtain high capacity VLC networks. Additionally, the OFDM technique has been proved to be a feasible candidate to obtain these high-speed networks [20], demonstrating impressive experimental data rates for short-range communications [27, 28].

Therefore, it appears to be clear that combining OFDM technique and imaging reception could be an interesting research field for the future. Table 3 shows the main parameters of a simulation scenario in which MIMO-OFDM, based on imaging reception, is evaluated. Fig. 9 illustrates the images of the LED arrays on the pixelated imaging receiver at two different positions in the room at a height of 0.75 m, which have been obtained by using a paraxial optic approach, as in the work by Zeng et al. [29]. The performance results of the multi-user LS receiver for these two positions of the detector array are compared in Fig. 10. In order to carry out a fair comparison, the BER performance is shown versus the maximum SNR observed at the receiving pixels for the emissions from the lamp  $l = 6$ , which is located the furthest from the detector, when this is positioned close to the corner (Fig. 9(b)), i.e.  $\max(\text{SNR}_j^{(l=6, \text{pos}=b)})$ ,  $j = 1, \dots, P$ . Here, the case labelled as  $L = 6$  is referred to the aggregate system BER (considering those of all the users  $l = 1, \dots, L$  jointly). Regarding those labelled as  $L = 1$ , they represent the single-user performances for the user  $l = 6$  (the worst). Finally,  $P_{\min}$  denotes the number of receiving channels (pixels) required for a correct joint demodulation, which is always 8 (those illuminated by the lamps, see Fig. 9). We can observe that the detector, when located close to a corner, requires more than 40 dB in the SNR to make the BER drop below  $10^{-6}$  when considering the aggregate performance. This represents a SNR loss of roughly 20 dB with respect to its corresponding single-user scenario. In contrast, evaluated under the same illumination conditions (versus the maximum  $\text{SNR}_j^{(l=6, \text{pos}=b)}$ ), the receiver at the centre of the room requires more than 15 dB less electrical power to obtain the same aggregate performance. Although these SNR values could be practical in a VLC

Parameter	Value
Room size (length $\times$ width $\times$ height):	7.5 m $\times$ 5.5 m $\times$ 3.5 m
Number of LED arrays:	6 (3 $\times$ 2)
Number of LEDs per array:	3600 (60 $\times$ 60)
Dimensions of each LEDs array:	1.2 m $\times$ 1.2 m
Positions of LED arrays (central point) ( $x, y, z$ ):	array 1: (1.50,1.50,3.50) array 2: (3.75,1.50,3.50) array 3: (6.00,1.50,3.50) array 4: (1.50,4.00,3.50) array 5: (3.75,4.00,3.50) array 6: (6.00,4.00,3.50)
LED lambertian order ( $n$ )	1
LED transmission bandwidth	$\sim$ 15 MHz
Total number of subcarriers ( $N$ )	64
Number of information subcarriers ( $S_I$ )	48
Number of bits per subcarrier ( $B$ )	4 (16-QAM)
OFDM symbol period ( $T_S$ )	4 $\mu$ s
Cyclic prefix extension ( $N_e$ )	16
Aggregate throughput	288 Mbit/s
Imaging lens f-number ( $f_{\#}$ )	1
Lens diameter ( $D$ )	4 cm
Number of pixels or receiving channels ( $P$ )	16 (4 $\times$ 4)
Detector size (silicon area)	1.6 cm $\times$ 1.6 cm

**Table 3.** Parameters for simulation

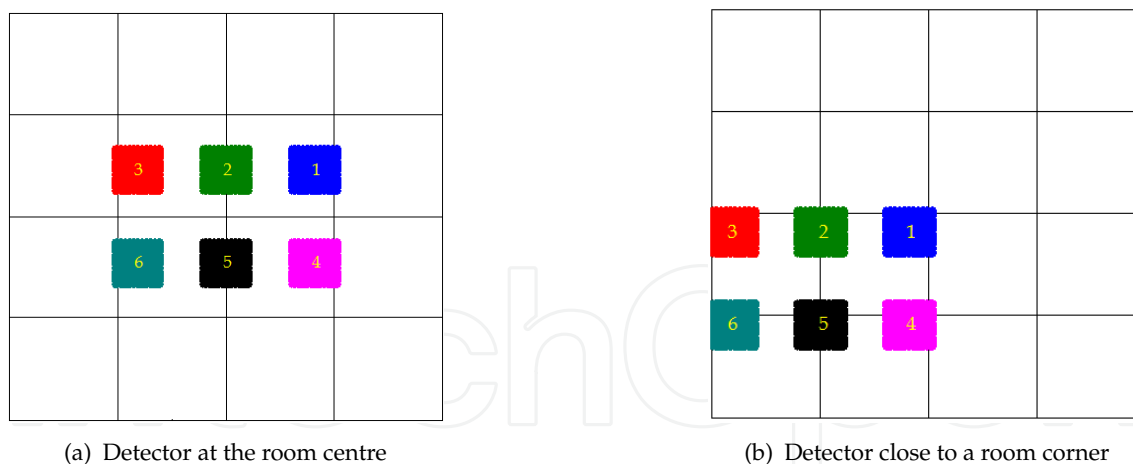


**Figure 9.** Images of the LED arrays on the detector at two positions

environment, it is evident that moving towards corners degrades enormously the aggregate performance due to the long distances and low inclination of the rays coming from the furthest lamps. Hence, it would be a more efficient solution to employ higher-order modulation modes (greater values of  $B$ ) for the lamps closer to the receiver and lower ones for those further away, even deactivating them as necessary, by using adaptive OFDM schemes [9]. In any case, what seems apparent, according to these preliminary results, is that MIMO-OFDM with imaging reception is a promising technique, which is worthy of further work.

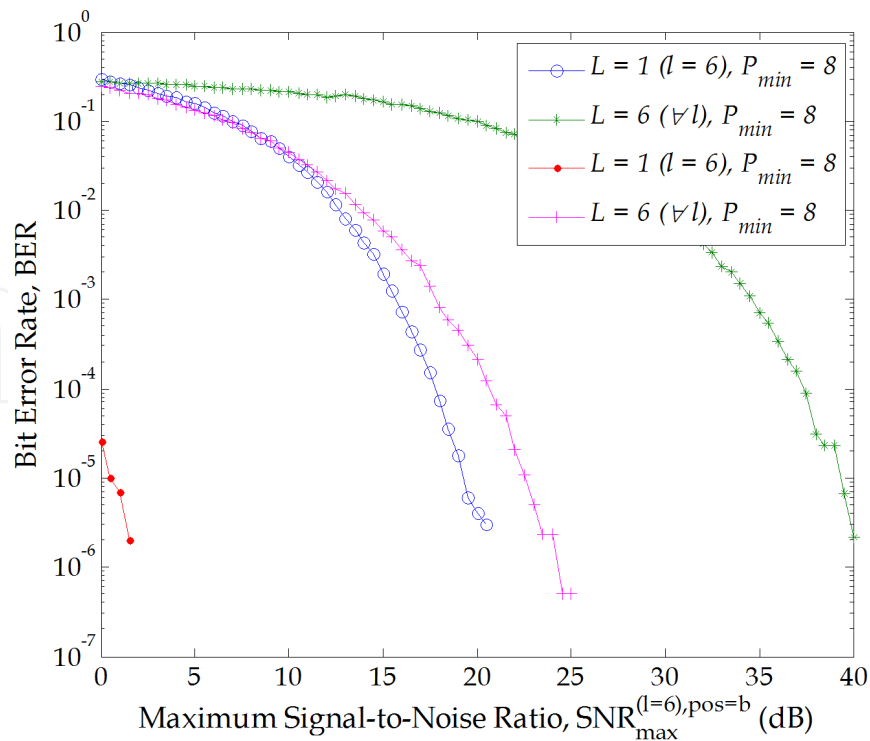


**Figure 10.** Performance comparison of multi-user LS detection based on imaging reception for two positions of the detector array

## 7. Conclusions

In this chapter, the employment of multi-user LS detection in conjunction with angle-diversity receivers and OFDM modulation technique for wireless optical communication has been evaluated. The MIMO optical channel model, which can be determined by using Monte Carlo-based ray-tracing algorithms, has been described in detail. This algorithm allows us to determine LOS and multiple-bounce reflection contributions to the received optical power at the photodetector, which enables a more accurate analysis of the proposed system performance. The multi-user detector, which is based on the linear combining of the incoming signals at its receiving branches, is shown to have a performance very close to that of the optimum ML detector. Additionally, it has been observed that strategies to find the truly significant receiving branches, during the data retrieving for a specific user, can be applied to reduce the complexity of the demodulation problem while maintaining and, even improving, the system performance. The results have also shown that aggregate high data rates can be obtained for indoor wireless optical communications at practical signal-to-noise ratios. Finally, the proposed multi-user OFDM system has been assessed for a visible-light communication scenario, where imaging reception is assumed. The preliminary results show that the previous scheme is an attractive candidate for developing high-capacity VLC networks, but further research still needs to be carried out.

## Acknowledgments

This work has been funded in part by the Spanish Research Administration (TEC2009-14059-C03-02), by the Canary Government (SolSubC200801000306) and the Plan E (Spanish Economy and Employment Stimulation Plan).

## Author details

Oswaldo González

Dept. Fundamental and Experimental Physics, Electronics and Systems  
University of La Laguna, Spain

## 8. References

- [1] Al-Ghamdi, A. G. & Elmirghani, J. M. H. [2004]. Analysis of diffuse optical wireless channels employing spot-diffusing techniques, diversity receivers, and combining schemes, *IEEE Transactions on Communications* 52(10): 1622–1631.
- [2] Alsaadi, F. E. & Elmirghani, J. M. H. [2009a]. Adaptive mobile line strip multibeam MC-CDMA optical wireless system employing imaging detection in a real indoor environment, *IEEE Journal on Selected Areas in Communications* 27(9): 1663–1675.
- [3] Alsaadi, F. E. & Elmirghani, J. M. H. [2009b]. Performance evaluation of 2.5 Gbit/s and 5 Gbit/s optical wireless systems employing a two dimensional adaptive beam clustering method and imaging diversity detection, *IEEE Journal on Selected Areas in Communications* 27(8): 1507–1519.
- [4] Armstrong, J. [2009]. OFDM for optical communications, *Journal of Lightwave Technology* 27(3): 189–204.
- [5] Barry, J. R., Kahn, J. M., Krause, W. J., Lee, E. A., & Messerschmitt, D. G. [1993]. Simulation of multipath impulse response for wireless optical channels, *IEEE Journal on Selected Areas in Communications* 11(3): 367–379.
- [6] Djahani, P. & Kahn, J. M. [2000]. Analysis of infrared wireless links employing multibeam transmitter and imaging diversity receivers, *IEEE Transactions on Communications* 48(12): 2077–2088.
- [7] Elgala, H., Mesleh, R. & Haas, H. [2011]. Indoor optical wireless communication: potential and state-of-the-art, *IEEE Communications Magazine* 49(9): 56–62.
- [8] González, O., Pérez-Jiménez, R., Rodríguez, S., Rabadán, J. & Ayala, A. [2005]. OFDM over indoor wireless optical channel, *IEE Proceedings-Optoelectronics* 152(4): 199–204.
- [9] González, O., Rodríguez, S., Pérez-Jiménez, R., Delgado, F. & Ayala, A. [2007]. Multi-user adaptive orthogonal frequency-division multiplexing system for indoor wireless optical communications, *IET Optoelectronics* 1(2): 68–76.
- [10] González, O., Rodríguez, S., Pérez-Jiménez, R., Mendoza, B. R. & Aayala, A. [2011]. Comparison of Monte Carlo ray-tracing and photon-tracing methods for calculation of the impulse response on indoor wireless optical channels, *Optics Express* 19(3): 1997–2005.
- [11] Grubor, J., Randel, S., Langer, K.-D. & Walewski, J. W. [2008]. Broadband information broadcasting using LED-based interior lighting, *Journal of Lightwave Technology* 26(24): 3883–3892.
- [12] Hanzo, L., Münster, M., Choi, B.-J. & Keller, T. [2003]. *OFDM and MC-CDMA for broadband multi-user communications, WLANs and broadcasting*, John Wiley & Sons, West Sussex, England.
- [13] IEEE Std 802.15.7 [2011]. IEEE standard for local and metropolitan area networks—part 15.7: Short-range wireless optical communication using visible light, pp. 1–309.
- [14] Jivkova, S. & Kavehrad, M. [2001]. Receiver designs and channel characterization for multi-spot high-bit-rate wireless infrared communications, *IEEE Transactions on Communications* 49(12): 2145–2153.
- [15] Kahn, J. M. & Barry, J. R. [1997]. Wireless infrared communications, *Proceedings of IEEE* 85(2): 265–298.

- [16] Kahn, J. M., You, R., Djahani, P., Weisbin, A. G., Teik, B. K. & Tang, A. [1998]. Imaging diversity receivers for high-speed infrared wireless communication, *IEEE Communications Magazine* 36(12): 88–94.
- [17] Komine, T., Lee, J. H., Haruyama, S. & Nakagawa, M. [2009]. Adaptive equalization system for visible light wireless communication utilizing multiple white LED lighting equipment, *IEEE Transactions on Wireless Communications* 8(6): 2892–2900.
- [18] Komine, T. & Nakagawa, M. [2003]. Integrated system of white LED visible-light communication and power-line communication, *IEEE Transactions on Consumer Electronics* 49(1): 71–79.
- [19] Komine, T. & Nakagawa, M. [2004]. Fundamental analysis for visible-light communication system using LED lights, *IEEE Transactions on Consumer Electronics* 50(1): 100–107.
- [20] Li, X., Vučić, J., Jungnickel, V. & Armstrong, J. [2012]. On the capacity of intensity-modulated direct-detection systems and the information rate of ACO-OFDM for indoor optical wireless applications, *IEEE Transactions on Communications* 60(3): 799–809.
- [21] Lomba, C. R., Valadas, R. T. & de Oliveira Duarte, A. M. [1998]. Experimental characterisation and modelling of the reflection of infrared signals on indoor surfaces, *IEE Proceedings-Optoelectronics* 145(3): 191–197.
- [22] Mesleh, R., Elgala, H. & Haas, H. [2011]. Optical spatial modulation, *IEEE/OSA Journal of Optical Communications and Networking* 3(3): 234–244.
- [23] Minh, H. L., O'Brien, D. C., Faulkner, G. E., Zeng, L., Lee, K., Jung, D., Oh, J. & Won, E. T. [2009]. 100-Mb/s NRZ visible light communications using a postequalized white LED, *IEEE Photonics Technology Letters* 21(15): 1063–1065.
- [24] O'Brien, D. C., Minh, H. L., Faulkner, G. E., Zeng, L., Lee, K., Jung, D. & Oh, J. [2008]. High-speed visible light communications using multiple-resonant equalization, *IEEE Photonics Technology Letters* 20(15): 1243–1245.
- [25] O'Brien, D. C., Zeng, L., Minh, H. L., Faulkner, G. E., Walewski, J. W. & Randel, S. [2008]. Visible light communications: challenges and possibilities, *Proceedings of IEEE 19th International Symposium on Personal, Indoor and Mobile Radio Communications, PIMRC 2008*, pp. 1–5.
- [26] Proakis, J. G. [2001]. *Digital Communications*, McGraw-Hill International Edition, Singapore.
- [27] Vučić, J., Kottke, C., Habel, K. & Langer, K.-D. [2011]. 803 Mbit/s visible light WDM link based on DMT modulation of a single RGB LED luminary, *Proceedings of Optical Fiber Communication Conference and Exposition, and the National Fiber Optic Engineers Conference (OFC/NFOEC) 2011*, pp. 1–3.
- [28] Vučić, J., Kottke, C., Nerreter, S., Langer, K.-D. & Walewski, J. W. [2010]. 513 Mbit/s visible light communications link based on DMT-modulation of a white LED, *Journal of Lightwave Technology* 28(4): 3512–3518.
- [29] Zeng, L., O'Brien, D. C., Minh, H. L., Faulkner, G. E., Lee, K., Jung, D., Oh, J. & Won, E. T. [2009]. High data rate multiple input multiple output (MIMO) optical wireless communications using white LED lighting, *IEEE Journal on Selected Areas in Communications* 27(9): 1654–1662.